Distinction between Effects of *IR*-Drop and Negative Capacitance of Fast Cyclic Voltammograms

Yuanyuan Liu , Koichi Jeremiah Aoki , Jingyuan Chen *

Posted Date: 16 August 2023

doi: 10.20944/preprints202308.1186.v1

Keywords: IR-drop; negative capacitance; double layer capacitance; fast scan cyclic voltammograms; microelectrode reactions

Article

Distinction between Effects of *IR*-Drop and Negative Capacitance of Fast Cyclic Voltammograms

Yuanyuan Liu [1], Koichi Jeremiah Aoki [2] and Jingyuan Chen [2,*]

[1] Department of Applied Physics, University of Fukui, Fukui, 910-0017, Japan; lyd21003g.u-fukui.ac.jp
[2] Electrochemistry Museum, Japan; d930099@yahoo.co.jp
* Correspondence: jchen@u-fukui.ac.jp; Tel.: +81-9082625425

Abstract: Diffusion-controlled cyclic voltammograms at fast scan rates show peak shifts as well as decreases in the peak currents from the predicted diffusion-controlled currents especially when currents are large in low concentration of supporting electrolyte. This has been conventionally recognized as an *IR*-drop effect by solution resistance on the peaks as well as heterogeneous kinetics. It is also brought about by negatively capacitive currents associated with charge transfer reactions. The reaction product generates dipoles with counterions to yield a capacitance, of which current flows oppositely to that of the double layer capacitance. The three effects are specified here in the oxidation of a ferrocenyl derivative by fast scan voltammetry. The expression for voltammograms complicated with *IR*-drop is derived analytically, and yields deformed voltammograms. The peak shift is approximately linear with the *IR*-term, but exhibits a convex variation. Dependence of some parameters on the peaks by the *IR*-drop is compared with those by the negative capacitance. The latter is more conspicuous than the former under conventional conditions. The two effects cannot be distinguished specifically except for variations of conductance of the solution.

Keywords: *IR*-drop; negative capacitance; double layer capacitance; fast scan cyclic voltammograms; microelectrode reactions

1. Introduction

Linear sweep cyclic voltammetry has been conventionally made at scan rates v ranging $0.01 < v < 0.2$ V s^{-1}. The slowest scan has been used on the assumption of the steady state for hydrodynamic voltammetry [1] and microelectrode voltammetry [2]. It often provides a well-defined voltammogram but takes a long period of a few minutes. An advantage of the slow scan rates is to distinguish faradaic, diffusion-controlled currents from background currents by a double layer capacitance (DLC). For example, the diffusion current at concentration 0.5 mM (M = mol dm^{-3}) redox species is roughly $I_d = 3v^{1/2}$ μA at a 1 mm^2 planar electrode for v in the unit of V s^{-1}. In contrast, a DLC of a platinum electrode in aqueous solutions, being $C = 30$ μF cm^{-2}, provides the capacitive current $I_c = 0.3v$ μA. Since the ratio is $I_c/I_d = 0.1\ v^{1/2}$, the diffusion currents at $v = 0.2$ V s^{-1} can be distinguished from the background with 5 % errors. A disadvantage is a time-consumed measurement, during which redox species might be altered through chemical complications. If faradaic reactions occur under an adsorbed state, the advantage is not perceptive because the background current has the same v-dependence as I_c. Slow responses fail to detect kinetic properties.

Study on homogeneous and heterogeneous kinetics requires such a wide range of v that reaction rates can be covered. A range of the kinetics is often much wider than the conventional scan rates (0.01 – 0.2 V s^{-1}), and hence fast scan voltammetry is desirable for kinetic work principally [3–10] and practically [11–14] for applications to neurotransmitter detection. Unfortunately, the increase in scan rates is associated with at least five problems to be considered. (A) *IR*-drop, in which applied voltage is lost by solution resistance, makes voltammograms deformed and shifted in a scanned direction [15,16]. (B) Even if difference in v-dependence of I_d and of I_c enables us to evaluate I_d accurately [17], the adsorption-controlled current, I_a, prohibits the extraction of I_a from the observed current because of the same v-dependence as I_c. (C) A delay of a potentiostat underestimates true currents at short time [**Error! Bookmark not defined.**,**Error! Bookmark not defined.**,**Error! Bookmark not defined.**].

Preprints (www.preprints.org) | NOT PEER-REVIEWED | Posted: 16 August 2023 doi:10.20944/preprints202308.1186.v1

(D) Heterogeneous kinetics represented by the Butler-Volmer equation makes the peak potential shifted and the peak current deviated lower than the predicted diffusion-controlled peak current [18] with an increase in v. (E) Fast scans more than 0.5 V s^{-1} generate the negatively capacitive current, which is caused by formation of dipoles of a reaction product with counterions at an electrode [19–23].

A level of these problems depends on magnitude of v. We suggest three classes; v < 0.2 V s^{-1}, v < 5 V s^{-1} and v < 500 V s^{-1}. Advantages and possible risks for each class are listed in Table 1.

Table 1. Advantages and risks for three classes for the levels

Range of v	Advantages	Risks
(I) < 0.2 V s^{-1}	Small background currents Easy extraction of diffusion currents Usage of low-cost potentiostats Possibility of theoretical analysis	Misleading kinetic reaction mechanisms Time consumption
(II) < 5 V s^{-1}	Possibility of subtraction of *IR*-drop Possibility of determining reaction mechanisms Evaluation of heterogeneous kinetics Comparison of the results with those by other rapid electrochemical methods Commercially available potentiostats	Discussion required for peak shifts Deformation of waveform Limitation to microelectrodes in order to prevent large currents
(III) < 500 V s^{-1}	Detection of kinetics with milli-second orders such as neurotransmitters	Empirical search for detecting conditions A loss of theoretical support

The usage of fast scan rates prevents clear distinction of faradaic reactions from backgrounds. The difficulty in the distinction in class III has been overcome with efforts of trial and error, as exemplified with the rapid detection of neurotransmitters [**Error! Bookmark not defined.–Error! Bookmark not defined.**]. The developed techniques are specific to given redox species under limited conditions. In contrast, those in class II have been carried out on the theoretical base of the difference in the v-dependence when faradaic reactions proceed in diffusion-control. If problems (A)-(E) are intertwined complicatedly, corrections are not enough sufficient for finding expected behavior of the faradaic waves. For class I, the intertwinement is largely solved except for adsorption in the v-dependence.

We examine here subjects (A)-(E) carefully. Since no stereotyped redox species has been found for the Butler-Volmer kinetics yet [24], (D) may be excluded from the present work on ferrocenyl derivatives [25–27]. If we pay attention only to diffusion-controlled currents under category (II), subjects (B) and (C) have been automatically resolved. Both (A) and (E), being necessarily involved in fast scan voltammetry, exhibit similar behavior in spite of different concepts. We examine in this work how voltammetric peak potentials and currents belonging to class (II) are varied with controlling parameters for (A) and (E) by use of fast scan voltammetry of a ferrocenyl derivative. Unfortunately, effects of *IR*-drop (A) have not been discussed systematically yet. Thus, we present here the experimental results and the theory.

2. Materials and Methods

2.1. Chemicals

All the chemicals were of analytical grade. Solutions were prepared in doubly distilled water prepared by CPW-100 (Advance, Tokyo, Japan). Aqueous solutions with different concentrations of

 doi:10.20944/preprints202308.1186.v1

KCl (0.005, 0.05, 0.1, 0.5 and 5 M) were prepared at the aim of varying solution resistance. The electrochemical charge transfer species was 1 mM (ferrocenylmethyl)trimethyl ammonium (FcTMA).

2.2. Voltammetry

Voltammetry was made in a three-electrode cell equipped with a working platinum wire electrode 0.03 mm, 0.5 mm in diameter or a 1.6 mm disk electrode. The tip of the wire was inserted into the solution by a given length (ca. 1 mm) which was measured with a microscope. The wire was not sealed with any insulator to expose an active area in order to avoid floating capacitance at crevices of electrode|insulator. The electrode was pretreated by being socked in the mixed acid (0.26 M acetic + 0.33 M nitric acid + 0.73 M phosphoric acid) for 1 min to clean the surface. A counter electrode was a platinum coil. A reference electrode was a homemade Ag|AgCl (*x* M KCl). A columnar porous glass was fixed to a tip of taper glass tube with a heat shrink tube, into which a Ag|AgCl wire was inserted together with *x* M KCl solution. In order to detect any leakage of chloride ions during the experiment, we measured the resistance values of the solution before and after the experimental test, which were almost the same.

A delay of the potentiostat, Compactstat by Ivium (Netherlands), was examined by using a carbon resistance 1 kΩ for a dummy cell by applying the voltage with 1 V. The maximum difference in the currents at the forward and the reverse scan was 3% at 8 V s^{-1}. Our voltammetry for FcTMA and various concentrations of KCl was made at scan rate less than 7 V s^{-1}. Ac-impedance was made for the 10 mV amplitude and frequency domain from 1 Hz to 10 kHz. All measurements were made at temperature of 25 ± 1 ℃.

3. Results

Figure 1A shows voltammograms at the 0.5 mm platinum wire electrode inserted in 1 mm length in the solution of 1.0 mM FcTMA + 5 mM KCl for several scan rates. FcTMA or related ferrocenyl derivatives have been recognized as such fast charge transfer reacting species that voltammetric peak potentials, E_p, may be independent of voltammetric scan rates [**Error! Bookmark not defined.**,**Error! Bookmark not defined.**,28–30]. However, the peak potential in Figure 1A shifted in the forward direction at the fast scan rates. The potential shift has often been attributed to the *IR*-drop. The resistance values were estimated from the inverse slope of the line connecting the peaks (solid lines) [**Error! Bookmark not defined.**,**Error! Bookmark not defined.**]. The slope for the anodic waves was the same as that for the cathodic one. This equality partially supports the effect of *IR*-drop on the potential shift. The inverse slope was close to the resistance (2.7 kΩ) obtained through Nyquist plots by ac-impedance. The potential at which the lines are extrapolated to zero current can be regarded as the peak potential without *IR*-drop. The difference between the extrapolated anodic potential and the cathodic one was 60 mV, indicating the diffusion- controlled behavior [**Error! Bookmark not defined.**]. The voltammograms in Figure 1B at the disk electrode 1.6 mm in diameter were drawn out to exhibit the peak-connecting line with the inverse slope of 5.5 kΩ, which was larger than the resistance value of 4.2 kΩ by ac-impedance. Except for this point, the behavior was almost the same as in (A).

Preprints (www.preprints.org) | NOT PEER-REVIEWED | Posted: 16 August 2023 doi:10.20944/preprints202308.1186.v1

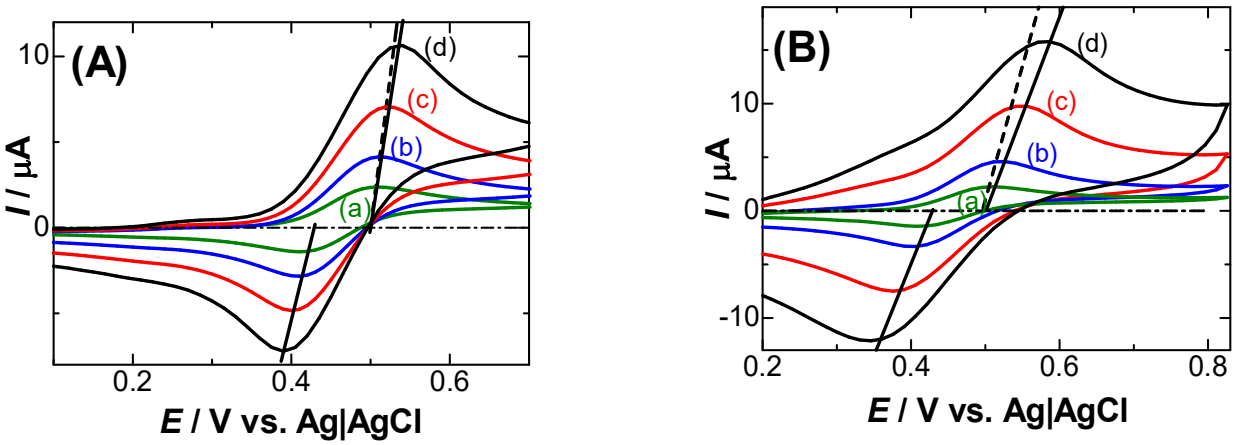

Figure 1. Voltammograms in 1.0 mM FcTMA + 5 mM KCl at the (A) Pt wire 0.5 mm in diameter and 1 mm long, (B) 1.6 mm disk Pt for v = (a) 0.03, (b) 0.1, (c) 0.3 and (d) 0.7 V s^{-1}. The solid lines are connecting lines on the peaks, while the dashed lines are drawn from the solution resistance by ac-impedance.

There may be a reason for the larger values of the slopes of voltammetric peaks than the R_s-values by ac-impedance. Figure 2 shows logarithmic plots of two kinds of the resistance against concentrations of KCl. R_s-values (a, b) by ac-impedance were linear with the logarithmic form of [KCl] with the slope –0.91, independent of the electrode geometry. The approximately inverse proportion of R_s to [KCl] agrees with the concept of ionic mobility by electric field [31]. The deviation of the slope (–0.91) from the ideal one (–1.0) can be attributed to the frequency dispersion of the double layer capacitance, of which values increase slightly with salt concentrations [**Error! Bookmark not defined.**,32,33]. It can be understood in terms of an upward shift of Nyquist plots with an increase in salt concentrations [**Error! Bookmark not defined.**]. It is noteworthy to pay attention to the invalidity of simple RC-relaxation of the double layer capacitances [**Error! Bookmark not defined.**,**Error! Bookmark not defined.**]. In contrast, the resistances evaluated from voltammetric peaks (c, d) were kept almost constant for the low salt concentrations. They are provided through the oxidation current of FcTMA rather than the capacitive currents of the electric double layer. The potential-shifts only caused by faradaic reactions can be attributed to effects of (i) electric migration [34–36], (ii) the heterogeneous kinetics for the charge transfer reaction [**Error! Bookmark not defined.**], (iii) following chemical reactions [37,38], and (iv) the negative capacitance associated with the charge transfer reaction [**Error! Bookmark not defined.**–**Error! Bookmark not defined.**]. We attempt to estimate these effects briefly here.

Preprints (www.preprints.org) | NOT PEER-REVIEWED | Posted: 16 August 2023 doi:10.20944/preprints202308.1186.v1

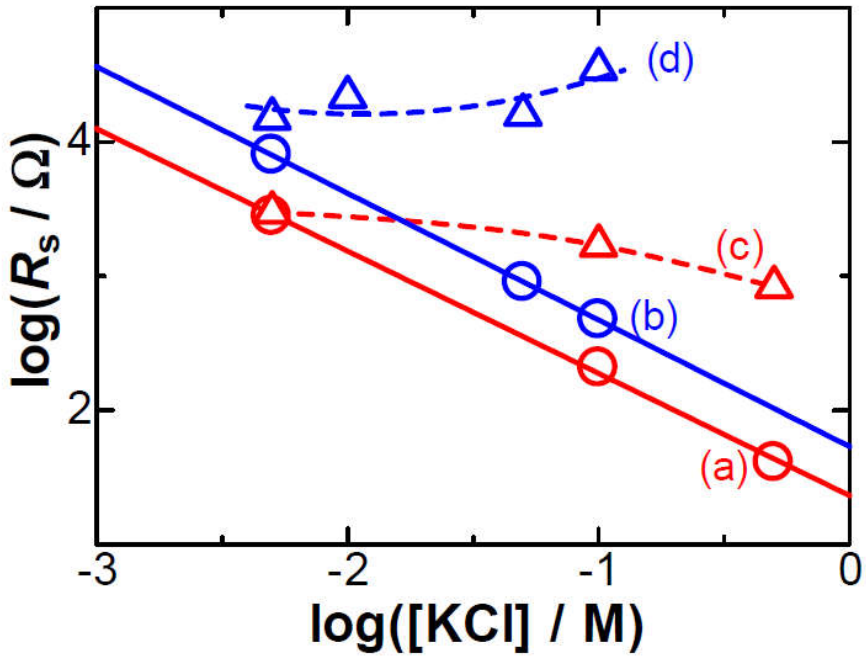

Figure 2. Logarithmic dependence of the solution resistance, *R*s on [KCl] at Pt wires (a, c) 0.5 mm and (b, d) 0.03 mm in diameter 1 mm in length. *R*s (a, b) were obtained by ac-impedance at the polarized potential, whereas (c, d) were obtained from slopes of lines connecting voltammetric peaks in Figure 1.

(i) The flux of a uni-valent cationic redox species controlled both with diffusion and electric migration is expressed by the Nernst-Planck equation, $j/F = -D\mathrm{d}c/\mathrm{d}x - (DF/RT)c(\mathrm{d}\phi/\mathrm{d}x)$ [39], where c is its concentration, D is the diffusion coefficient, and ϕ is the potential in solution at a distance from the electrode x. It can be approximated to be $j/F = -Dc^*/\delta - (DF/RT)c^*(\Delta\phi/\delta)$, on the basis of a concept of diffusion layer [40]. Here, its thickness at the peak current, I_P, is given by $\delta = Dc^*FA/I_P$, where A is the electrode area. The ratio of the current component of the migration to that of diffusion is $(F/RT)\Delta\phi$. When $\Delta\phi$ is replaced by R_sI_P, the ratio becomes less than 0.5 % under our experimental conditions. Therefore, migration has no contribution to the potential shift in our case.

(ii) The electrode kinetics has often caused potential shifts. A quantitatively accessible kinetics is represented by the Butler-Volmer equation. The theoretical peak currents and potentials for different scan rates can be obtained from the analytical equation at a given transfer coefficient α and a heterogeneous rate constant k^0 [**Error! Bookmark not defined.**]. Figure 3c–e shows the variation of I_P with E_P for several scan rates at the $\alpha = 0.5$ and some values of k^0 by use of our software of the kinetics so that I_P vs. E_P were close to the experimental ones (a). However, the experimental plots (a) is different from theoretical variations for any different values of k^0. The inconsistency was also applied to other values of R_s (b). Since no potential shift was found in 0.1 M KCl solution (b), it is not reasonable to explain the shift in terms of the heterogeneous kinetics. However, the explanation only by the kinetics has often been reported [**Error! Bookmark not defined.–Error! Bookmark not defined.**].

(iii) A following chemical reaction causes a potential shift, as can be understood from the Nernst equation for reaction rates faster than voltammetric rates. Ferrocenyl compounds, however, are not satisfied with the condition of the rates, and hence, item (iii) is unsuitable of explaining the present potential shifts.

(iv) The negative capacitance is brought about through the following steps in Figure 4: a charge transferred redox species (Fc) is coupled with a counterion (Cl^-) for electric neutrality by responding to the externally applied field E_{ap} to yield an electric dipole(Fc^+-Cl^-); the dipole with the dipole moment p is oriented in the direction for enhancing the external field by $-pc/\varepsilon_0$ to yield the effective field E_{ef}, which generates a capacitance with a sign opposite to a double-layer capacitance [**Error!**

Preprints (www.preprints.org) | NOT PEER-REVIEWED | Posted: 16 August 2023 doi:10.20944/preprints202308.1186.v1

Bookmark not defined.,41]. The negative capacitance has been obtained for ferrocenyl derivative [**Error! Bookmark not defined.**,**Error! Bookmark not defined.**], ruthenium complex, iridium complex [**Error! Bookmark not defined.**] and hemin [**Error! Bookmark not defined.**] by ac-impedance. Since the voltammetric current from the negative capacitance is proportional to the scan rate, it depresses the diffusion tail to cause the potential shift [**Error! Bookmark not defined.**]. The negative capacitance varies with electrode areas and scan rates, as the *IR*-drop does. The similarity in the properties stimulates us to distinguish their properties theoretically.

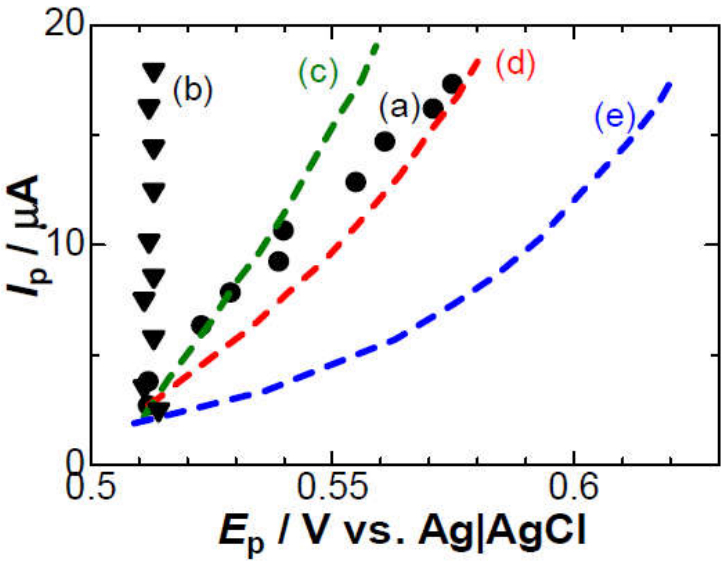

Figure 3. Variations of I_p against E_p at the 0.5 mm Pt wire electrode 1 mm long in the solution of 1.0 mM FcTMA + (a) 0.005 M and (b) 0.1 M KCl at $0.03 < v < 3$ V s^{-1}. The other plots were calculated from the Butler-Volmer typed kinetic equation for the k^0 = (c) 0.01, (d) 0.005 and (e) 0.001 cm s^{-1} and $\alpha = 0.5$.

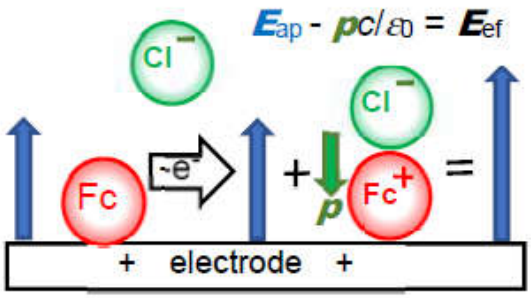

Figure 4. Illustration of generation of a dipole with Cl^- just after the oxidation of the ferrocenyl molecule.

4. Theory of effects of *IR*-drop

The electrode reaction here is a simple Nernstian charge-transfer reaction with the mass transfer controlled by x-directional diffusion. The diffusion coefficient of the reduced species, D, is assumed to have a common value to the oxidized species. Letting the solution resistance between a working electrode and a reference one be R_s, the scan rate be v and the initial potential be E_{in}, we can express the linearly scanned potential participating efficiently in the oxidation for the current I as $E(t) = E_{in} + vt - I(t)R_s$ at the time t. The common value of D implies that the sum of concentrations of both species is equal to the bulk concentration, c^*, in any time and any location. Thus, the Nernst equation for the reduced species tends to

Preprints (www.preprints.org) | NOT PEER-REVIEWED | Posted: 16 August 2023 doi:10.20944/preprints202308.1186.v1

$$c_{x=0} = c^*/\{1 + \exp((E_{in} + vt - I(t)R_s)F/RT)\} \quad (1)$$

On the other hand, the surface concentration is given by a solution of the diffusion equation [**Error! Bookmark not defined.**] as a function of the current density j

$$c_{x=0} = c^* - F^{-1}(\pi t)^{-1/2}\int_0^t j(t-u)u^{-1/2}\mathrm{d}u$$

Inserting this equation into Equation (1) and extracting j by the technique previously described [42] yields

$$j/c^*FD^{1/2} = \mathrm{d}\int_0^t (\pi u)^{-1/2}\{1 + \exp[-(E(t-u)F/RT]\}^{-1}\mathrm{d}u / \mathrm{d}t \quad (2)$$

Application of Leibniz's theorem [43] makes the combination of the integral and the differentiation be reduced to

$$I/Ac^*FD^{1/2} = (1/4)\int_0^t \{\pi(t-u)\}^{-1/2}\{\mathrm{sech}^2(E(u)F/2RT)\}\{v - R_s\mathrm{d}I(u)/\mathrm{d}u)\}(F/RT)\,\mathrm{d}u$$

where A is the area of the electrode.

We replace the time by the potential through $y = (E_{in} + vu)F/RT$, and define the dimensionless current as

$$f(t) = I(t)/I_{p0} \quad (3)$$

where I_{p0} is the peak current without solution resistance, given by $I_{p0} = 0.446Ac^*F(FDv/RT)^{1/2}$. The current has the dimensionless parameter for the resistance

$$\rho = I_{p0}R_sF/RT \quad (4)$$

and can be rewritten as

$$f(t) = \pi^{-1/2}\int_{\zeta_{in}}^{\zeta_{ap}} (\zeta_{ap} - y)^{-1/2}g(y - 2.24\rho f(y))\{1 - \rho\mathrm{d}f(y)/\mathrm{d}y\}\,\mathrm{d}y \quad (5)$$

where $g(x) = (1/4)\mathrm{sech}^2(x/2)$, and ζ_{in} and ζ_{ap} are the dimensionless initial voltage $E_{in}F/RT$ and the dimensionless applied voltage $(E_{in}+vt)F/RT$, respectively. Function f was evaluated by numerical computation by discretization of $\zeta_{ap}-\zeta_{in} = nh$ for a small value of h, as was described in the supporting information.

Figure 5 shows dimensionless voltammograms for several values of resistance parameter ρ (Equation (4)). With an increase in the values of ρ, voltammograms shift in the positive direction accompanied with a decrease in the peak currents. An exemplified value of $\rho = 4$ corresponds to I_{p0} = 0.1 mA, R_s = 1 kΩ.

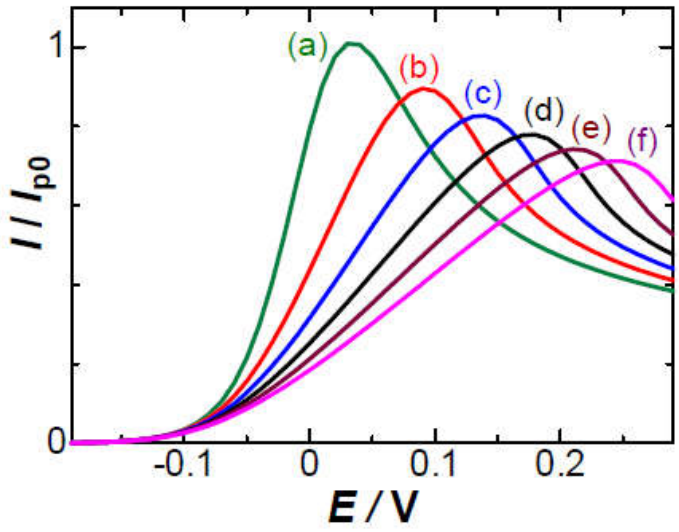

Preprints (www.preprints.org) | NOT PEER-REVIEWED | Posted: 16 August 2023 doi:10.20944/preprints202308.1186.v1

Figure 5. Voltammograms computed from Equation (5) for ρ = (a) 0, (b) 2, (c) 4, (d) 6, (e) 8 and (f) 10.

Peaks were calculated for various values of ρ. The E_p increased from 0.029 V convexly with ρ, as shown in Figure 6a. The intuitively predicted increase in E_p is $I_{p0}R_s$ or (26 mV)ρ,

$$(E_p)_{IR,prdct} = I_{p0}R_s + 0.026 \text{ V} \quad (6)$$

as shown in the line of Figure 6b. The tangent line at $\rho = 0$ has the slope, 33 mV (Figure 6c). The slight shift from 26 mV is ascribed to the smaller decrease in the current for $E > E_p$ than that for $E < E_p$ (see Figure 5) owing to the diffusion tail. Consequently, the E_p-values calculated from Equation (5) for $\rho < 3$ are larger than the line (Equation (6)). Since the variable ρ is proportional to $v^{1/2}$ through I_{p0}, the effect of *IR*-drop on the voltammograms is approximately exhibited in the form of the linearity of E_p to $v^{1/2}$ rather than log v.

The peak current normalized with the theoretically diffusion-controlled one decreased with an increase in the resistance, as shown in Figure 7. The decrease can be explained in terms of the following reasons: the shift of the peak potential delays the arrival at the peak; the delay is equivalent to a substantial decrease in the applied scan rate, v_{ap}, which leads a decrease in I_p so that $I_p < I_{p0} = k_1 v_{ap}^{1/2}$, where $k_1 = 0.446Ac^*F(FD/RT)^{1/2}$. By letting the effective scan rate, v_{ef}, be $I_p = kv_{ef}^{1/2}$, v_{ef} decreases with ρ, as shown on the right ordinate in Figure 7b. It varies linearly with $\rho^{1/2}$. The effective rate becomes less than a half for $\rho > 10$ or $I_{p0}R_s > 0.25$ V. The difference, 0.446– $(I_p/Ac^*F)(RT/FDv_{ap})^{1/2}$, was approximately proportional to $\rho^{1/2}$. As a result, the peak current at any value of R_s can be approximated as

$$I_p/I_{p0} = 1 - 0.09\rho^{1/2} \quad (7)$$

This is a new insight for the *IR*-drop effect that has not been reported yet [**Error! Bookmark not defined.**,**Error! Bookmark not defined.**]. Since ρ is proportional to $v^{1/2}$ through I_{p0} (Equation (4)), the peak current for the *IR*-drop can be approximated as $I_p = kv^{1/2} - k_1v^{3/4}$.

It is interesting to compare the effects of *IR*-drop on I_p and E_p with those of the negative capacitance (NC), C_{rx}. The E_p due to C_{rx} has varied linearly with $\log[(\sigma^*/c^*)^2(v/FRTD)]$ [**Error! Bookmark not defined.**] for $E_p - E^o > 0.06$ V, where σ^* is the sum of the surface charge density of the oxidized and the reduced species, and c^* is the bulk concentration of FcTMA. In contrast, its variation for $E_p - E^o < 0.1$ V is linear with $(\sigma^*/c^*)(v/FRTD)^{1/2}$, as shown in Figure 6 on the upper abscissa, which was scaled so that the line may be overlapped with the line for the *IR*-drop. The line can be approximated as $0.0217(\sigma^*/c^*)(v/FRTD)^{1/2} + 0.03$ in the unit of V for $E_p - E^o > 0.06$ V. The empirical equality, $C_{rx} = 0.16(F/RT)\sigma^*$, in Equation (13) of ref. **Error! Bookmark not defined.** can substitute C_{rx} for σ^* to give

$$(E_p)_{NC,\,<0.10V} / \text{V} = 0.135(C_{rx}/Fc^*)(RTv/FD)^{1/2} + 0.03 \quad (8)$$

When potential shift is small, the observed shift is the sum of the shifts for the *IR*-drop and the negative capacitance,

$$(E_p)_{<0.10V} / \text{V} = 0.135(C_{rx}/Fc^*)(RTv/FD)^{1/2} + 1.15I_{p0}R_s + 0.03 \quad (9)$$

R_s varies with geometry of electrodes at given conductivity of solution. A disk electrode makes R_s be $1/4\Lambda[\text{KCl}]a = (\pi/A)^{1/2}/4\Lambda[\text{KCl}]$ [44] for the molar conductivity Λ of KCl. R_s at a wire electrode, on the other hand, is inversely proportional to A. Some variables that control E_p are summarized in Table 2 for comparing these two effects.

Table 2. Variations of E_p and I_{p0}- I_p with four variables.

variables	E_p		I_{p0}- I_p	
	IR	NC	*IR*	NC
c^*	c^*	1	$c^{*3/2}$	c^*
A(disk)	$A^{1/2}$	1	$A^{5/4}$	A

Preprints (www.preprints.org) | NOT PEER-REVIEWED | Posted: 16 August 2023 doi:10.20944/preprints202308.1186.v1

v	$v^{1/2}$	$v^{1/2}$	$v^{3/4}$	v
R_s	R_s	1	$R_s^{1/2}$	1

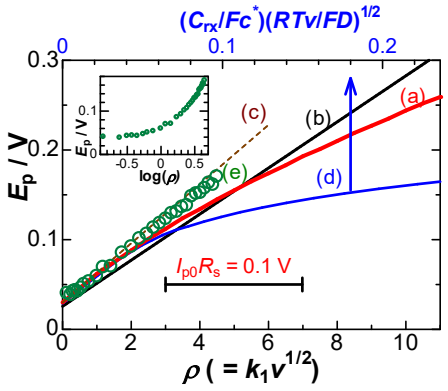

Figure 6. Variations of the peak potential by (a) the *IR*-drop with the resistance parameter, (b) the intuitive *IR*-drop by $I_{p0}R_s$, (c) the tangent line of (a) at ρ = 0, (d) the negative capacitance with $(C_{rx}/c^*)(v/RTFD)^{1/2}$, and (e) experimental variations of E_p with ρ where R_s = 2.7 kΩ in 1mM FcTMA + 5 mM KCl at the 0.5 mm wire electrode.

The *IR*-drop contribution normalized with I_{p0} is

$$(I_{p0} - I_p)/I_{p0} \equiv X_{IR} = 0.09(I_{p0}R_sF/RT)^{1/2} \quad (10)$$

On the other hand, the negatively capacitive peak current is given by $I_{NC} = I_{p0} - AC_{rx}v$. The normalized contribution is given by

$$X_{NC} = AC_{rx}v/\ I_{p0} \quad (11)$$

Eliminating I_{p0} from Equations (10) and (11) yields

$$X_{IR} = 0.09(AR_sC_{rx}vF/RTX_{NC})^{1/2} \quad (12A)$$

Especially, the relation for the disk is given by

$$(X_{IR})_{disk} = 0.06A^{1/4}(C_{rx}vF/RT\Lambda[KCl]X_{NC})^{1/2} \quad (12B)$$

Figure 8 shows variations of $(X_{IR})_{disk}$ with X_{NC} for some electrode areas at conventionally experimental conditions of v, κ (=Λ[KCl]) and C_{rx}. The constant of $X_{IR}^2X_{NC}$ indicates that the effect of the negative capacitance is predominant to that of the *IR*-drop. Furthermore, high scan rates at large electrodes in low salt concentration should enhance both the *IR*-drop and the negative capacitance.

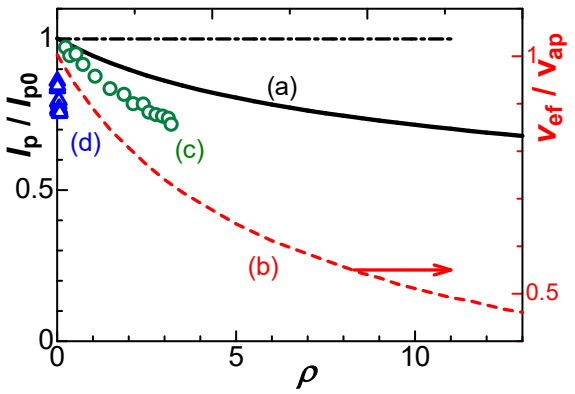

Preprints (www.preprints.org) | NOT PEER-REVIEWED | Posted: 16 August 2023 doi:10.20944/preprints202308.1186.v1

Figure 7. Variations of (a) the peak current (b) the ratio of effective scan rate and (c) the experimental peak current with the dimensionless resistance ρ at (circles) R_s=2.7 kΩ and (triangles) R_s= 80 Ω.

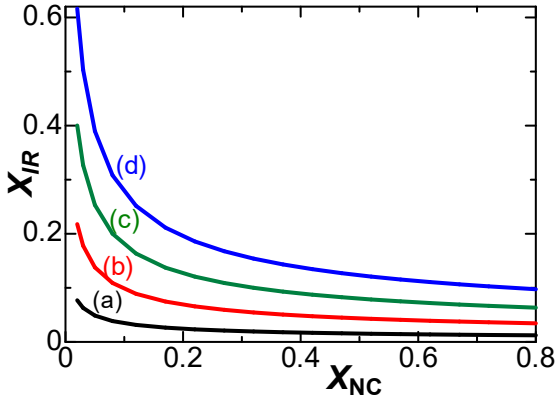

Figure 8. Variations of the fraction of the *IR*-drop, X_{IR} (= $(I_{p0} - I_p)/I_{p0}$), with that of the negative capacitance, X_{NC}, for A = (a) 0.01, (b) 0.04, (c) 0.09 and (d) 0.16 mm² at v = 0.1 V s^{-1}, κ = 0.133 S m^{-1} corresponding to [KCl] = 10 mM, and C_{rx} = 50 μF cm^{-2}.

5. Discussion

Experimental values of E_p in the solution of 1 mM FcTMA + 5 mM KCl were plotted against ρ (= I_pR_sF/RT) in Figure 6e, where the value of R_s for ρ was obtained from the Nyquist plot. They were on a line, deviated upward from the theoretical curve Figure 6a of the *IR*-drop, and hence the potential shift cannot be ascribed only to the *IR*-drop. The plot of the experimental E_p vs. log v is shown in the inset of Figure 6, as is often plotted. The non-linearity indicates that the conventionally observed linearity should not explain any *IR*-drop effect. Addition of voltages does not agree with that of processes because of non-linear relation to voltages in electrochemical processes. The experimentally obtained ratio, I_p/I_{p0}, decreased with an increase in v, as shown in Figure 7c,d at two values of R_s. The variation of the triangular marks is close to that of the circles if ρ-axis is expanded. The experimental values (c,d) lower than the theory (a) were caused by the effect of the negative capacitance.

It is current that can make arithmetic operations possible through an addition of current at a parallel process or of inverse currents at a series one. In order to confirm the dependence of the *IR*-drop contribution on the scan rates, we plotted I_{p0}–I_p in solution of 1 mM FcTMA + 5 mM KCl against v logarithmically in Figure 9a. The plot shows a line with the slope, 0.71, which is close to the theoretical value, 3/4, in Table 2. The value of the slope suggests the control of the *IR*-drop. On the other hand, the currents at the 0.03 mm wire in 0.1 M KCl (in Figure 2d) did not contain any *IR*-drop effect, as demonstrated in Figure 3b. The logarithmic plots of I_{p0}–I_p vs. v shows a line with slope of 0.92 in Figure 9b. The value of the slope is close to unity, and hence it should belong to the negative capacitance.

Preprints (www.preprints.org) | NOT PEER-REVIEWED | Posted: 16 August 2023 doi:10.20944/preprints202308.1186.v1

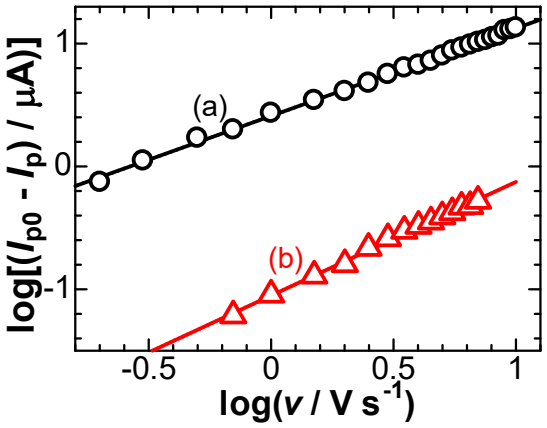

Figure 9. Logarithmic variation of I_{p0}-I_p with v in the solution of (a) 1 mM FcTMA + 0.005 M KCl at the 0.5 mm wire electrode (b) 1 mM FcTMA + 0.1 M KCl at the 0.03 mm wire electrode.

6. Conclusion

Fast scan for a diffusion-controlled voltammogram makes the peak potential shifted and the peak current decreased from the theoretical values. The deviation is not caused by the Butler-Volmer typed kinetics but is caused by combinations of *IR*-drop of solution resistance and the negative capacitance associated with electrode reactions. The two effects are hardly discriminated in terms of scan rate-dependence, but the distinction can be made with variation of concentrations of electrolytes or size of electrodes. The effect of the negative capacitance is likely to appear more strongly than the *IR*-drop effect in voltammetric peaks. Wire electrodes less than 0.05 mm in diameter are suitable for suppressing the *IR*-drop effects even in low concentrations of electrolytes.

The expression for voltammograms complicated by the *IR*-drop is given by a non-linear integral equation as a function of $I_{p0}R_s$. The evaluation has to relay on numerical computation through digitization. The peak potential shifts intuitively by $I_{p0}R_s$. However, the theory predicts that it shows a non-linear relation with $I_{p0}R_s$, because of asymmetric waveform near the peak. Calculated potential shifts over 0.2 V are smaller than the values of $I_{p0}R_s$. The potential shift retards the time reaching the peak, yielding a decrease in the actual scan rate. As a result, the peak current is observed to be suppressed.

6. Supporting information

This section informs numerical computation of

$$f(t) = \pi^{-1/2}\int_{\zeta_{in}}^{\zeta_{ap}} (\zeta_{ap} - y)^{-1/2} g(y - 2.24\rho f(y))\{1-\rho df(y)/dy\}\, dy \qquad (5)$$

Discretization of $\zeta_{ap}-\zeta_{in} = nh$ with an equal width h rewrites Equation (5)

$$f(t) = \pi^{-1/2}\Sigma_{k=0}^{n-1} \int_{\zeta_{in}+kh}^{\zeta_{in}+(k+1)h} (\zeta_{ap}-y)^{-1/2} g(y - 2.24\rho f(y))\{1 - \rho df(y)/dy\}\, dy \qquad (S1)$$

It is assumed that $g(y - 2.24\rho f(y))$ and $\{1 - 2.24\rho df(y)/dy\}$ are constant at each discretized domain, $g(y - 2.24\rho f(y)) \approx g(y_k - 2.24\rho f(y_k)) = g(y_k - 2.24\rho f_k)$

$$1- 2.24\rho df(y)/dy\} \approx 1 - 2.24\rho(y_{k+1} - y_{k-1})/2h$$

Then (S1) becomes

$$f_n = \pi^{-1/2}\Sigma_{k=0}^{n-1} g(y_k - 2.24\rho f_k)\{1 - 2.24\rho(f_{k+1} - f_{k-1})/2h\} \int_{\zeta_{in}+kh}^{\zeta_{in}+(k+1)h} (\zeta_{ap} - y)^{-1/2} dy \qquad (S2)$$

The integral provides

Preprints (www.preprints.org) | NOT PEER-REVIEWED | Posted: 16 August 2023 doi:10.20944/preprints202308.1186.v1

$$\int_{\zeta in+kh}^{\zeta in+(k+1)h} (\zeta_{ap} - y)^{-1/2} dy = \int_{(n-k-1)h}^{(n-k)h} x^{-1/2} dx = 2h^{1/2}\{(n-k)^{1/2} - (n-k-1)^{1/2}\}$$

Then, (S2) can be rewritten as

$$f_n = 2(h/\pi)^{1/2} \Sigma_{k=0}^{n-1} H_{k,n}$$

$$H_{k,n} = g(y_k - 2.24\rho f_k)\{1 - 2.24\rho(f_{k+1} - f_{k-1})/2h\}\{(n-k)^{1/2} - (n-k-1)^{1/2}\}$$

We attempted to calculate f_n successively starting for $n = 1$ on the assumption of replacing f_n in $H_{n,n}$ as f_{n-1}, we found that values of f_n diverged before a voltammetric peak. The assumption was refined by by extracting f_n from $H_{n,n}$ to rewrite the following form:

$$f_n = 2(h/\pi)^{1/2} [g(y_{n-1} - 2.24\rho f_{n-1})\{1 - 2.24\rho(f_n - f_{n-2})/2h\} + \Sigma_{k=0}^{n-2} H_{k,n}] \quad (S3)$$

Solving Equation (S3) with respect to f_n yields

$$f_n = 2(h/\pi)^{1/2}[g(y_{n-1} - 2.24\rho f_{n-1})\{1+2.24\rho f_{n-2}/2h\} + \Sigma_{k=0}^{n-2} H_{k,n}]$$

$$/ [1+(\pi h)^{-1/2} 2.24\rho\, g(y_{n-1} - 2.24\rho f_{n-1})] \quad (S4)$$

The initial value was $f_0 = 0$ for $y_0 = \zeta_{in}$ and $f_{-1} = 0$ because of no current.

References

1. A.J. Bard. L.R. Faulkner, Electrochemical Methods; Fundamentals and Applications, John Wiley & Sons, New York, 2nd. Ed., 2001, pp. 331–332.
2. A.J. Bard. L.R. Faulkner, Electrochemical Methods; Fundamentals and Applications, John Wiley & Sons, New York, 2nd. Ed., 2001, pp. 170–176.
3. J.O. Howell, J.M. Goncalves, C. Amatore, L. Klasinc, R.M. Wightman, J.K. Kochi, J. Am. Chem. Sot., 1984, 106, 3968.
4. C. Amatore, C. Lefrou, J. Electroanal. Chem., 1990, 296, 335–358.
5. M.I. Montenegro, D. Pletcher, J. Electroanal. Chem., 1986, 200, 371.
6. A. Fitch, D.H. Evans, J. ElectroanaI. Chem., 1986, 202, 83.
7. C. Amatore, E. Maisonhaute, G. Simonneau, Electrochem. Commun., 2000, 2, 81–84
8. C.P. Andrieux, D. Garreau, P. Hapiot, J. Pinson, J.M. Saveant, J. Eleetroanal. Chem., 1988, 243, 321–335.
9. G. Wosiak, D. Coelho, E. B. Carneiro-Neto, E. C. Pereira, M. C. Lopes, Anal. Chem., 2020, 92, 15412-15419.
10. C. Amatore, A. Oleinick, I. Svir, Anal. Chem., 2008, 80, 7947-7956.
11. J.G. Roberts, L.A. Sombers, Anal. Chem. 2018, 90, 490–504.
12. J.E. Baur, E.W. Kristensen, L.J. May, D.J. Wiedemann, R.M. Wightman, Anal. Chem., l988, 60, 1268–1272.
13. B.J. Venton, Q. Cao, Analyst, 2020, 145, 1158.
14. P. Puthongkham, B.J. Venton, Analyst, 2020, 145, 1087–1102.
15. BioLogic, EC-Lab – Application Note #41, 07/2012, CV Sim: Simulation of the simple redox reaction (E) Part II: The effect of ohmic drop and double layer capacitance.
16. K.J. Aoki, J. Chen, Tips of Voltammetry, IntehOpen, 2018, pp. 1–19.
17. K.J. Aoki, J. Chen, Y. Liu, B.Jia, J. Electroanal. Chem., 2020, 856, 113609.
18. H. Matsuda, Y. Ayabe, Z. Elektrochmie. 1955, 59, 494–503.
19. K.J Aoki, J. Chen, X. Zeng, Z. Wang, RSC Adv. 2017, 7, 22501–22501.
20. K.J. Aoki, J. Chen. P. Tang, J. Phys. Chem. C, 2018, 122, 16727–16732.
21. K.J. Aoki, J. Chen, R. Wang, Electroanalysis, 2019, 31, 1–9.
22. K.J. Aoki, T. Peng, J. Chen, Am. J. Anal. Chem., 2019, 10, 286–295.
23. R. Wang, K.J. Aoki, J. Chen, Electrochem, 2022, 3, 397–406.
24. K.J. Aoki, C. Zhang, J. Chen, T. Nishiumi, J. Electroanal. Chem., 2013, 706, 40–47.
25. P. Sun, M.V. Mirkin, Anal. Chem., 2006, 78, 6526–6534.
26. J. Velmurugan, P. Sun, M. V. Mirkin, J. Phys. Chem. C, 2009, 113, 459–464.
27. J. F. Smalley, S. W. Feldberg, C. E. D. Chidsey, M. R. Linford, M. D. Newton, Y.-P. Liu, J. Phys. Chem., 1995, 99, 13141–13149.
28. N. Nioradze, J. Kim, S. Amemiya, Anal. Chem., 2011, 83, 828–835.

29. Y. Li, D. Bergman, B. Zhang, Anal. Chem., 2009, 81, 5496–5502.
30. Y. Zhang, J. Zhou, L. Lin, Z. Lin, Electroanal., 2008, 20, 1490–1494.
31. P. Atkins, J.de Paula, Atkin's Physical Chemistry, 10th ed., Oxford University Press, pp, 799–802.
32. K. J. Aoki, R. He, J. Chen, Electrochem, 2021, 2, 71–82.
33. K.J. Aoki, R. He, J. Chen, Electrochem, 2021, 2, 631–642.
34. Y. Zhou, P. Yang, C. Yuan, Y. Huo, Chem. Eng. Trans., 2013, 33, 559–564.
35. R.S. Sorbello, Mater. Res. Soc. Conference Proceedings 1996, 427, 73–81.
36. B.R. Putra, K.J. Aoki, J. Chen, F. Marken, Langmuir, 2019, 35, 2055–2065.
37. P. Song, A.C. Fisher, J.D. Wadhawan, J.J. Cooper, H.J. Ward, N.S. Lawrence, RSC Adv., 2016, 6, 70237–70242.
38. H. M. Nassef, A.-E. Radi, C.K. O'Sullivan, Electrochem. Commun., 2006, 8, 1719–1725.
39. A.J. Bard. L.R. Faulkner, Electrochemical Methods; Fundamentals and Applications, John Wiley & Sons, New York, 2nd. Ed., 2001, pp. 29
40. A. Molina, J. Gonzalez, E. Laborda, R.G. Compton, Phys. Chem. Chem. Phys., 2013, 15, 2381–2388.
41. K.J Aoki, S. Taniguchi, J. Chen, Omega ACS, 2020, 5, 29447–29452.
42. K. Aoki, Electroanalysis, 2005, 17, 1379–1383.
43. M. Abramowitz, I.A. Stegun, Handbook of Mathematical Functions, National Bureau of Standards, 1964, pp. 11, 3.3.7.
44. J.S. Newman, Electrochemical Systems, Prentice-Hall Inc. Englewood Cliff, N. J. Chapter 18, pp. 340–345.